Theoretical study of wakefield acceleration of electrons in capillary Z-pinch plasma waveguide

A A Shapolov[1],*, B Fekete[1], M Kiss[1], S Szatmari[2] and S V Kukhlevsky[1]

[1]Department of Physics, University of Pecs, Pecs, Hungary
[2]Department of Experimental Physics, University of Szeged, Szeged, Hungary

*Email: sapolov@gamma.ttk.pte.hu

Abstract. The theoretical investigation of wakefield acceleration of electrons by CO_2-laser pulse with central wavelength of 10.6 μm and input peak intensity of $\sim 10^{17}$ W/cm^2 in transient hydrogen-plasma waveguide has been conducted. The plasma waveguide is produced by the fast Z-pinch discharge inside a 3 mm inner diameter and 50 mm long capillary. The waveguide properties of the capillary Z-pinch plasma were obtained from the space and frequency dependent wave equation that combines the attenuated charged particle inertia and the light wave effects in the plasma for the ideal Gaussian laser beam. For simulation of temporal and spatial evolution of electron density and other plasma variables during the capillary discharge, we used a standard one-fluid, two-temperature one-dimensional magnetohydrodynamic (MHD) model complemented with atomic data of hydrogen. Simulations showed that the guiding channel occurs far from capillary wall and exists for a few nanoseconds. In terms of laser driven plasma wakefield accelerators (LWFA), the Z-pinch waveguide is able to extend the acceleration length over the whole capillary, assuming that a single-mode transmission takes place. To quantify such ability of the channel, a correlation coefficient was introduced and computed at different input beam spot sizes. An optimal beam spot size was determined by taking maximum of time average of the coefficient over the channel lifetime. At the end of the guiding channel existence, the repetitive focusing and defocusing patterns were observed with intensity increase at the focal points. For simulation of the wakefield acceleration of electrons in the different waveguiding regimes we used the particle-in-cell (PIC) combined with the aforementioned MHD model. Influence of the waveguiding regimes on the electron acceleration was demonstrated.

1. Introduction

The waveguide effect of capillary discharge and its applications attract interest of many researchers [1-23]. The guiding of high intensity laser pulse has been widely used in laser driven plasma wakefield accelerators [1]. In the absence of guiding channel, the interaction length is basically limited by diffraction to the Rayleigh range [9]. In partially ionized plasmas, further limitation of the interaction length can be caused by ionization-induced refractive defocusing. Therefore, most of the researchers deal with hydrogen gas filled micro-capillary discharge waveguides [5-14], [16-22] in which the guiding core is extended to the capillary wall, i.e., the effects of the wall are inevitable. For example, the study [6] reported the variation of the pulse energy transmission during the ablating current and the temporal evolution of the transverse spatial profile of the exiting beam, as a result of many physical effects such as inverse bremsstrahlung, stimulated Raman scattering, stimulated Brillouin scattering, atomic modulation instabilities and the ionization of the discharge plasma loss mechanisms. Transient Z-pinch guiding channel was experimentally demonstrated in [5], where fully ionized He-plasma column generated in a capillary was used for channelling high-intensity ($>10^{17}$ W/cm^2) Ti:sapphire laser pulse. The Ar-plasma capillary waveguide was demonstrated in [15]. The Ar-plasma capillary

waveguide excited by Z-pinch was modelled in [15, 23]. The investigation of wakefield acceleration of electrons by laser pulse in plasma waveguides has been conducted in [16-21].

In this paper, we present the theoretical investigation of wakefield acceleration of electrons by CO_2-laser pulse with central wavelength of 10.6 μm and input peak intensity of $>10^{15}$ W/cm^2 in transient H-plasma waveguide. The plasma waveguide is produced by the fast Z-pinch discharge inside a 3 mm inner diameter and 50 mm long capillary. In Sec. 2, the waveguide properties of the capillary Z-pinch plasma were obtained from the space and frequency dependent wave equation that combines the attenuated charged particle inertia and the light wave effects in the plasma for the ideal Gaussian laser beam. For simulation of temporal and spatial evolution of plasma variables, during the capillary discharge, we used a standard one-fluid two-temperature one-dimensional MHD model [22, 23] complemented with atomic data of hydrogen (Sec. 2). Influence of the different waveguiding regimes on the wakefield acceleration of electrons was demonstrated in Sec. 3. For simulation of the wakefield acceleration of electrons we used the particle-in-cell (PIC) model [11-14] combined with the aforementioned MHD model (Sec. 3).

2. Waveguiding properties of the capillary Z-pinch plasma

Transverse electric field perturbations $\delta\vec{E}_t$ in plasma become light waves in the vacuum limit when the plasma effects are negligible. The inhomogeneous wave equation governing such perturbations can be written as

$$\nabla^2 \delta\vec{E}_t - \frac{1}{c^2}\frac{\partial^2 \delta\vec{E}_t}{\partial t^2} = \mu_0 \frac{\partial \delta\vec{J}_e}{\partial t} \qquad (1)$$

The inhomogeneous term $\delta\vec{J}_e$ represents the plasma effects. Because the EM waves in plasma are fast phenomena, we expect that the plasma response will be inertial. Thus, the current density perturbation in plasma induced by the electric field $\delta\vec{E}_t$ is given by $\delta\vec{J}_e = -en_e\delta\vec{v}_e$, where e is the electron charge, n_e is the electron density and $\delta\vec{v}_e$ is the electron velocity perturbation, respectively. The right-hand side of (1) can be rewritten as follows:

$$\frac{\partial \delta\vec{J}}{\partial t} \approx -en_e \frac{\partial \vec{v}_e}{\partial t}, \qquad (2)$$

Since the capillary Z-pinch dynamic is much slower compared to the perturbation caused by the electric field. The motion of an electron with charge e and mass m_e in response to the electric field is governed by

$$m_e \frac{\partial \delta\vec{v}_e}{\partial t} = -e\delta\vec{E}_t - m_e f_{ei}\delta\vec{v}_e \qquad (3)$$

where the last term on the right-hand side represents the impulse exchange between electrons and ions with a frequency f_{ei} in which the velocity of ions is neglected. Notice, we do not deal with the contribution of magnetic force. In that regard note, that the magnetic field of EM waves does not influence the magnitude of $\delta\vec{v}_e$ just change its direction. For electric field perturbations, we consider the wave solutions for ideal input Gaussian-beam $\delta\vec{E}_t(r,z,t) = \delta\tilde{\vec{E}}_t(r,z)\exp(i\omega t)$ in which $\delta\tilde{\vec{E}}_t(r,z)$ is space-dependent complex-valued electric field amplitude. For such perturbation, we expect a phase-shifted time harmonic inertial plasma response $\delta\vec{v}_e = \delta\tilde{\vec{v}}_e(r,z)\exp(i\omega t)$. Solving (3) basing on this form, we get the wave equation that combines the attenuated charged particle inertia and the light wave effects in a plasma:

$$\nabla^2 \delta\vec{E}_t - \frac{1}{c^2}\frac{\partial^2 \delta\vec{E}_t}{\partial t^2} - \frac{1}{c^2}\frac{\omega\omega_{pe}}{\omega - if_{ei}}\delta\vec{E}_t = 0 \qquad (4)$$

where $\omega_{pe} = (e^2 n_e/\varepsilon_0 m_e)^{1/2}$ is the electron plasma frequency. Using the proposed ideal input Gaussian-beam, (4) can be rewritten as the space- and frequency-dependent wave equation:

$$\left(c^2\nabla^2 + \omega^2\tilde{\varepsilon}_r\right)\delta\tilde{\vec{E}}_t(r,z) = 0 \qquad (5)$$

where $\widetilde{\varepsilon}_r = 1 - \omega^2 /(\omega^2 - i\omega f_{ei})$　is the relative permittivity of plasma, from which the refractive index is $\widetilde{n}_r = \widetilde{\varepsilon}_r^{1/2}$. Thus, the electric field of light wave in capillary Z-pinch determined by (4) and (5) depends on the refractive index of dynamically changing plasma channel via ω_{pe} and f_{ei}.

For the simulation of temporal and spatial evolution of the electron density and other plasma variables during the capillary Z-pinch discharge, we used a standard one-fluid, two-temperature, 1-D MHD model [22, 23]. In a cylindrical coordinate system. Equations of the model are as follows:

$$\frac{\partial n_i}{\partial t} + \frac{1}{r}\frac{\partial}{\partial r}\left(rv_r n_i\right) = 0 \tag{6}$$

$$m_i n_i \left(\frac{\partial v_r}{\partial t} + v_r \frac{\partial v_r}{\partial r}\right) = J_z \frac{\partial A_z}{\partial r} - \frac{\partial p}{\partial r} - \frac{1}{r}\frac{\partial}{\partial r}\left(r\pi_{rr}\right) + \frac{\pi_{\varphi\varphi}}{r} \tag{7}$$

$$\frac{3}{2}n_e\left(\frac{\partial T_e}{\partial t} + v_r \frac{\partial T_e}{\partial r}\right) = -\frac{p_e}{r}\frac{\partial}{\partial r}(rv_r) - \frac{1}{r}\frac{\partial}{\partial r}\left(rq_e^r\right) - \pi_e^{rr}\frac{\partial v_r}{\partial r} - \pi_e^{\varphi\varphi}\frac{v_r}{r} - \pi_e^{rz}\frac{\partial v_e^r}{\partial r} + Q_e \tag{8}$$

$$\frac{3}{2}n_i\left(\frac{\partial T_i}{\partial t} + v_r \frac{\partial T_i}{\partial r}\right) = -\frac{p_i}{r}\frac{\partial}{\partial r}(rv_r) - \frac{1}{r}\frac{\partial}{\partial r}\left(rq_i^r\right) - \pi_i^{rr}\frac{\partial v_r}{\partial r} - \pi_i^{\varphi\varphi}\frac{v_r}{r} + Q_i \tag{9}$$

$$-\frac{1}{r}\frac{\partial}{\partial r}\left(r\frac{\partial A_z}{\partial r}\right) = \mu_0 J_z \tag{10}$$

$$\frac{\partial J_z}{\partial t} + \frac{1}{r}\frac{\partial}{\partial r}\left(rv_r J_z\right) = \frac{e}{rm_e}\frac{\partial}{\partial r}\left(r\pi_{rz}\right) \tag{11}$$

$$n_e - \langle Z\rangle n_i = 0 \tag{12}$$

Here, n_e - electron density, n_i - ion density, v_r - plasma radial velocity, J_z - axial current density, T_e - electron temperature, T_i - ion temperature, $\langle Z\rangle$ - the average ion charge, $p = p_e + p_i$ - plasma pressure, Q_e - electron heating, Q_i - ion heating, A_z - the axial vector potential, $\pi_{\alpha\beta} = \pi_e^{\alpha\beta} + \pi_i^{\alpha\beta}$ - stress tensor, q_e^r - radial electron heat flow and q_i^r - radial ion heat flow. Spatial evolution of plasma variables are treated in Euler's specification of the flow field, whereas the total number of ions in capillary is constrained to be unchanged, i.e.

$$n_0 = \frac{p_0}{T_0} \equiv \frac{2}{R^2}\int_0^R rn_i dr \tag{13}$$

where R is the capillary radius, and n_0, p_0, T_0 are the initial neutral particle density, gas pressure and temperature, respectively. The electric current is assumed to be sinusoidal:

$$I(t) = I_{max}\sin\left(2\pi\frac{t}{T_{cur}}\right) \equiv 2\pi\int_0^R rJ_z dr, \tag{14}$$

where I_{max} and T_{cur} are the peak and cycle duration of the electric current, respectively. The system of equations (6)-(12) was solved for the boundary conditions corresponding to no-diffusive wall $\left(\partial n_i / \partial r\big|_{r=R} = 0\right)$, no-viscous wall $\left(\partial v_r / \partial r\big|_{r=R} = 0\right)$, in case of ions thermally insulated wall $\left(\partial T_i / \partial r\big|_{r=R} = 0\right)$ and in regards of electrons thermally conductive wall caused by magnetic pressure acting on electrons $\left(q_e^r \propto T_e J_z \left(\partial A_z / \partial r\right)\big|_{r=R} \neq 0\right)$. Nernst effect was also taken into consideration.

The general waveguiding properties of the capillary Z-pinch plasma have been derived for different gases. We have used plasma variables provided by the MHD model. The peak value of the current pulse, half-cycle duration, and the initial gas pressure were set to 30 kA, 100 ns and 0.6 mbar, respectively. The studies were conducted for CO_2-laser pulse with an input peak intensity of 10^{15} W/cm^2 and different spot sizes of $w_0 = 80 \dots 200$ μm. As an example, figure 1-4 illustrate evolution of the spatial and spectral intensity distributions of guided laser beam with optimal spot size of $w_0^{opt} = 134$ μm in Ne and Kr-plasma. The spatial distribution was computed at the central wavelength ($\lambda = 10.6$ μm) of CO_2-laser pulse. In case of spectral distribution, the evaluation was studied at the capillary axis. We found that higher frequency components of the guiding pulse propagate a bit faster resulting in a slight shape-distortion of pulse after a longer distance. The studies showed, that in the first few nanosecond of the guiding channel lifetime its single-mode transmission ability is fairly low, and this

time range varies with the applied beam spot size. A transient guiding channel is always emerging prior the maximum Z-pinch compression, independently of the used gases.
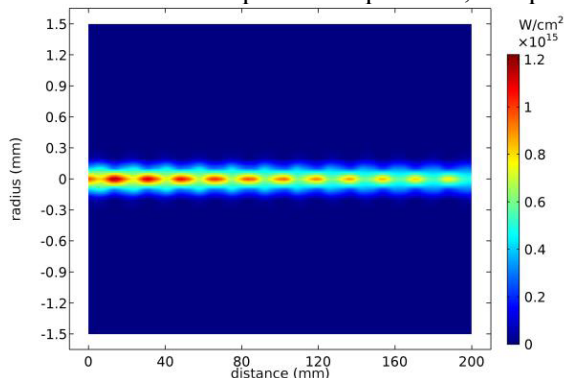

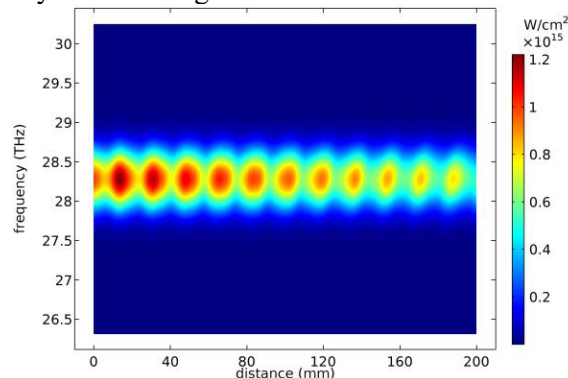**Figure 1.** The intensity distribution of guided laser beam in Ne-plasma.

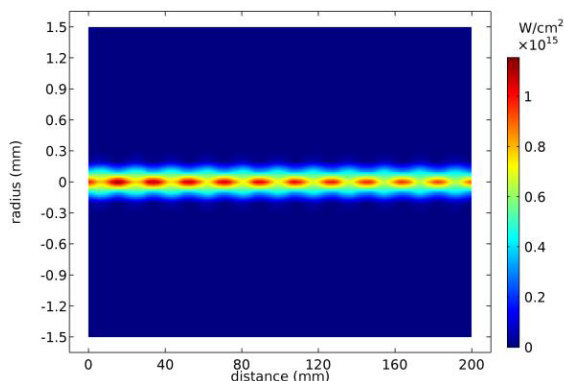**Figure 2.** The spectral distribution of guided laser beam in Ne-plasma.

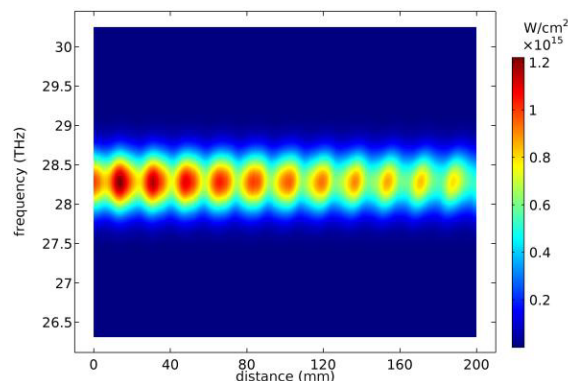**Figure 3.** The intensity distribution of guided laser beam in Kr-plasma.

Figure 4. The spectral distribution of guided laser beam in Kr-plasma.

In single-mode regime, the guiding channel is able to extend the interaction length (Rayleigh-range) over the whole capillary length. In this regime the shape distortion of propagated pulse is insignificant even after longer distances (>100 mm). In order to quantify ability of the channel to produce the single mode regime, a correlation coefficient [23] was computed at different input beam spot sizes. The optimal beam spot size w_0^{opt} = 134 μm was determined by taking maximum of time average of the coefficient over the channel lifetime. The ability of plasma channel to guide the high intensity laser pulse is a crucial tool in the LWFA. Dynamic of the electron density distribution in the capillary Z-pinch involves changes in channel transmission. Therefore, the relatively short existence of the guiding channel necessitates low timing jitter between the laser system and the Z-pinch discharge. In order to improve the transmission ability, two options may come up, namely, the timing jitter should be reduced further or the time-dependent channel radius should be followed by the matched spot size. When the guiding channel significantly shrinks, the input beam spot size exceeds the matched spot size, resulting the repetitive focusing and defocusing patterns. Intensity at the focal points can be higher as at the input (figure 1-4). Formation of the guiding channel strongly depends on rising time of the excitation current pulse amplitude of which can be decreased by using lighter gases.

For hydrogen, the waveguiding properties of plasma channel produced by the capillary Z-pinch are shown in figure 5 and 6. The computations were performed for I_{max} = 9.9 kA, T_{cur} / 2 = 47 ns and the initial pressure of hydrogen p_0 = 1.1 mbar. The studies were conducted for CO_2-laser pulse with duration of 0.5 ps and input peak intensity of 10^{17} W/cm² at the different spot sizes. As an example, figure 5 and 6 show evolution of the spatial and spectral intensity distributions of guided laser beam for w_0 = 150 μm.
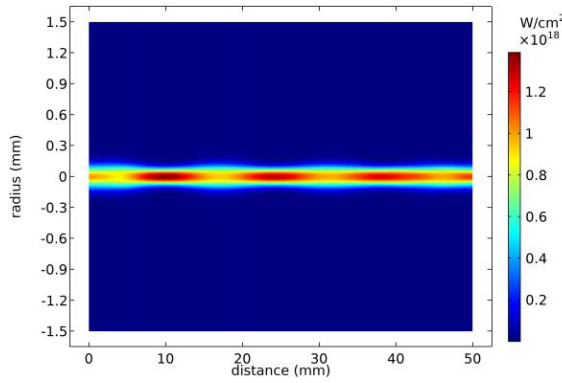
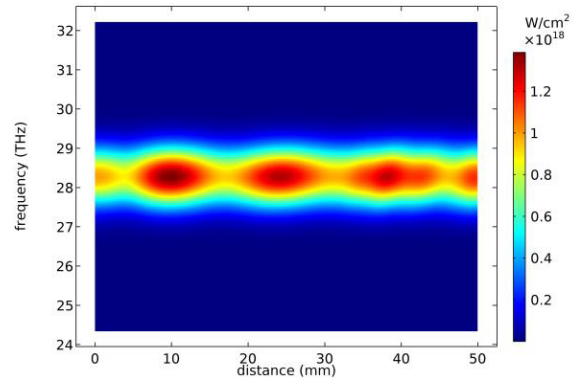**Figure 5.** The intensity distribution of guided laser beam in the H-plasma.

Figure 6. The spectral distribution of guided laser beam in the H-plasma.

3. Acceleration of electrons in capillary Z-pinch plasma waveguide

For simulation of the wakefield acceleration of electrons in hydrogen plasma channel produced by capillary Z-pinch, we used the particle-in-cell (PIC) model combined with the MHD model presented in Sec. 2. Newton's 2nd law for j-th electron with relativistic correction is given by

$$\frac{d}{dt}\left(m_e \gamma^j \vec{v}_e^j\right) = \vec{F}, \tag{15}$$

where m_e is the rest mass of electron, $\gamma^j = \left(1 - \vec{v}_e^{j2}/c^2\right)^{-1/2}$ is the relativistic factor and $\vec{F} = \vec{F}_e + \vec{F}_P$ is the force acting on electron. It is a superposition of two most dominant electric and ponderomotive forces:

$$\vec{F} = -e\vec{E} - \frac{e^2 \nabla \vec{E}_L^2}{4m_e \omega_0^2}. \tag{16}$$

Here, $\vec{E} = -\nabla U$ is the electric field caused by charge separation, $\vec{E}_L$ is the electric field amplitude of laser and ω_0 is the central angular frequency of laser pulse. Electric field caused by charge separation can be obtained from Gauss's law or Poisson's equation

$$\nabla \cdot \vec{E} = \rho/\varepsilon_0 \quad \text{or} \quad -\nabla^2 U = \rho/\varepsilon_0, \tag{17}$$

where $\rho = <Z>en_i - en_e$ is the charge density. In case of hydrogen plasma, $<Z> = 1$, i.e. $\rho = e(n_i - n_e)$. In the discrete case, the expression in bracket can be written as follows

$$\rho^d = e(N_i - N_e) = e\sum_{j=1}^{N} n_i \delta(\vec{r} - \vec{q}_i^j) - e\sum_{j=1}^{N} n_e \delta(\vec{r} - \vec{q}_e^j) \tag{18}$$

where $\vec{q}_e^j$ and $\vec{q}_i^j$ are the positions of j-th electron and ion. Correspondingly, $\vec{v}_e^j = d\vec{q}_e^j/dt$. All of equations above describing electron movement can be used for ions by interchanging m_e with m_i. Since $m_e \ll m_i$, ponderomotive force doesn't affect ions. Thus, they would "standing still" during whole process, i.e. $\vec{v}_i^j = 0$ and $\vec{q}_i^j = \vec{r}^j$. On the other hand, in hydrogen plasma $n_i = n_e = n$. Number of particles in a mesh volume at $\vec{r}$ position is $V_{mesh}(\vec{r}) = G_c(\vec{r})/n$, where $G_c(\vec{r})$ is the coupling constant which makes equality between discrete and continuous plasma frequency:

$$\omega_{pe}(\vec{r}) \approx \omega_{pe}^D(\vec{r}) = \sqrt{\frac{e^2}{\varepsilon_0 m_e} \sum_{j=1}^{N} \frac{G_c(\vec{r})}{V_{mesh}(\vec{r})} \delta(\vec{r} - \vec{q}_e^j)} \tag{19}$$

Now (18) can be rewritten as follows

$$\rho^d = e\sum_{j=1}^{N} \frac{G_c(\vec{r})}{V_{mesh}(\vec{r})} \left[\delta(\vec{r} - \vec{r}^j) - \delta(\vec{r} - \vec{q}_e^j)\right] \tag{20}$$

Combining all of results above we get system of equations of the PIC model:

$$\vec{v}_e^j = d\vec{q}_e^j/dt \tag{21}$$

$$\gamma^j = \left(1 - \vec{v}_e^{j2}/c^2\right)^{-1/2} \tag{22}$$

$$\frac{d}{dt}\left(m_e \gamma^j \vec{v}_e^j\right) = e\nabla U - \frac{e^2 \nabla \vec{E}_L^2}{4m_e \omega_0^2} \tag{23}$$

$$-\nabla^2 U = \frac{e}{\varepsilon_0} \sum_{j=1}^{N} \frac{G_c(\vec{r})}{V_{mesh}(\vec{r})}\left[\delta(\vec{r} - \vec{r}^j) - \delta(\vec{r} - \vec{q}_e^j)\right] \tag{24}$$

The electron density evolution computed by using the above presented PIC model was compared with the MHD-based density perturbation model which is formulated as follows. Continuity equation of mass density of electrons is given by

$$\frac{\partial \rho_e}{\partial t} + \nabla \cdot \rho_e \vec{v}_e = 0 \tag{25}$$

Introduction of perturbed term of mass density $_e = _{e0} + \delta_e$ yields

$$\frac{\partial \rho_{e0}}{\partial t} + \frac{\partial \delta\rho_e}{\partial t} + \nabla \cdot \rho_{e0}\vec{v}_e + \nabla \cdot \delta\rho_e \vec{v}_e = 0 \tag{26}$$

Since $\delta\rho e << \rho e0$ and $\delta\rho e$ varies much faster in time than ρ_{e0}, the first and the last terms of equation above can be neglected. Taking relativistic factor γ into account we get

$$\frac{\partial}{\partial t}\left(m_e \gamma \delta n_e\right) + n_{e0}\nabla\left(e\nabla U - \frac{e^2 \nabla \vec{E}_L^2}{4m_e \omega_0^2}\right) + \left(\frac{e}{m_e}\nabla U - \frac{e^2 \nabla \vec{E}_L^2}{4m_e \omega_0^2}\right)\cdot\nabla \cdot n_{e0} = 0 \tag{27}$$

In case of hydrogen plasma, the charge density   on the right-hand side of Poisson's equation (17) can be expressed as follows

$$\rho = e(n_i - n_e) = e(n_i - n_{e0} + \delta n_e) = e\delta n_e. \tag{28}$$

Here, $n_i - n_{e0} = 0$ due to plasma quasi-neutrality. Thus, we can do the following transformations on the 2nd term of (27):

$$\frac{n_{e0}}{m_e}\nabla\left(e\nabla U - \frac{e^2 \nabla \vec{E}_L^2}{4m_e \omega_0^2}\right) = \frac{e^2 n_{e0}}{\varepsilon_0 m_e \gamma}\gamma\delta n_e - \frac{e^2 n_{e0}}{4m_e^2 \omega_0^2}\nabla^2 \vec{E}_L^2 = \omega_{pe}^2 \gamma\delta n_e - \frac{e^2 n_{e0}}{4m_e^2 \omega_0^2}\nabla^2 \vec{E}_L^2 \tag{29}$$

where ω_{pe} is the relativistic plasma frequency, and is the relativistic factor for Gaussian laser beam, in which f_{ei} is the collisional frequency between electrons and ions. Combining all of results above we get the system of equations of density perturbation model that includes Eq. (30) and the following equations.

$$\gamma = \left(1 + \frac{e^2 \vec{E}_L^2}{2m_e^2 c^2 \left(\omega_0^2 + f_{ei}^2\right)}\right)^{1/2} \tag{30}$$

$$\left(\frac{\partial^2}{\partial t^2} + \omega_{pe}^2\right)\gamma\delta n_e = \nabla \cdot \left(\frac{e^2 n_{e0}}{4m_e^2 \omega_0^2}\nabla \vec{E}_L^2\right) - \frac{e}{m_e}\vec{E}\cdot\nabla n_{e0} \tag{31}$$

$$\nabla \cdot \vec{E} = -\frac{e}{\varepsilon_0}\delta n_e \tag{32}$$

Evolution of the electron density and energy gain during the acceleration was computed by using the above presented PIC for different waveguiding regimes, which occur at the propagation time of 0.60, 2.55, 7.05 and 8.80 ps (figure 7-10). Evolution of the electron density and energy gain during the acceleration was computed by using the above presented PIC for different wave-guiding regimes, which occur at the propagation time of 0.60, 2.55, 7.05 and 8.80 ps (figure 7-10).

Figure 11 shows evolution of the electron energy maximum, where the vertical lines indicate the local maxima, which are related to four different regimes. The respective spectra of electrons are shown in figure 12. We note that that acceleration of electrons is nonlinear versus the acceleration time (figure 11). We investigated correspondence of the electron energy maxima at the four regimes (figure 11) with the peaks of axial intensity of guided laser beam (figure 13). The respective transverse intensity distribution of guided laser beam is shown in figure 14. Comparison of figure 11 and 13 indicates quasi-synchronization of the local electron energy maxima with the inflection points between peaks of intensity of guided laser beam. The above presented PIC model (figure 7-10) was compared with the MHD-based density perturbation model (figure 15-18) in case of the same waveguiding regimes (0.60, 2.55, 7.05 and 8.80 ps). The PIC model provides information about energy gain during the acceleration (figure 11 and 12), while the perturbation model gives more exact information about

plasma frequency (figure 19). Plasma wavelength of the PIC model is about 200 μm (figure 9 and 10), while the exact value is 144 μm that corresponds to the plasma frequency $\omega_{pe} = (e^2 n_e / \varepsilon_0 m_e \gamma)^{1/2}$.
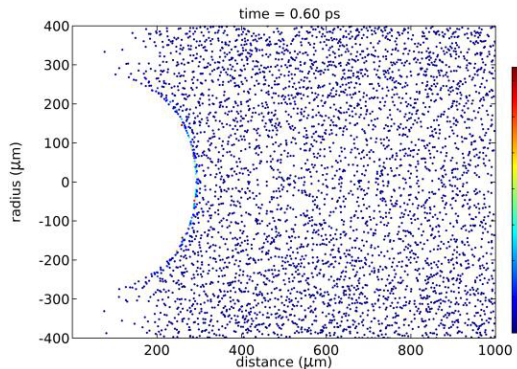

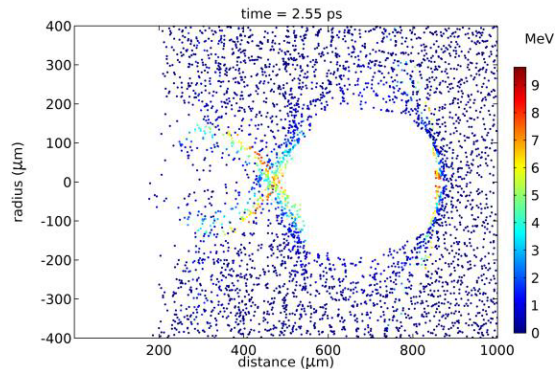**Figure 7.** Electron distribution at 0.60 ps.
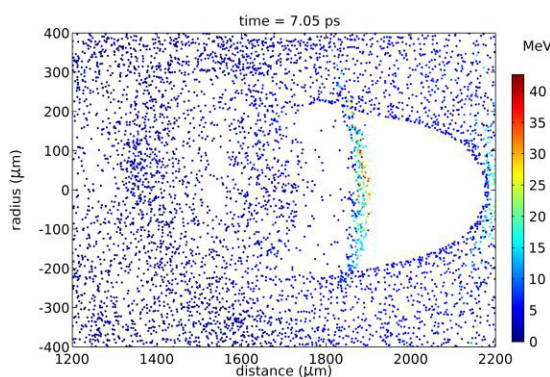

Figure 8. Electron distribution at 2.55 ps.
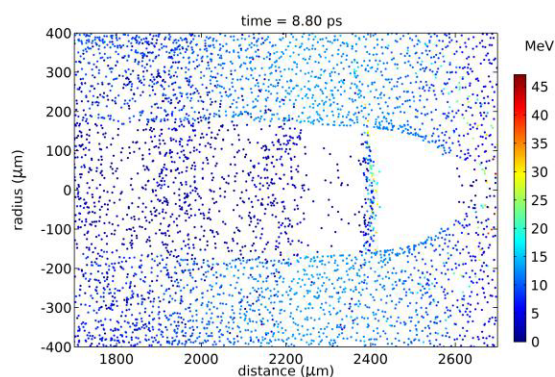

Figure 9. Electron distribution at 7.05 ps.
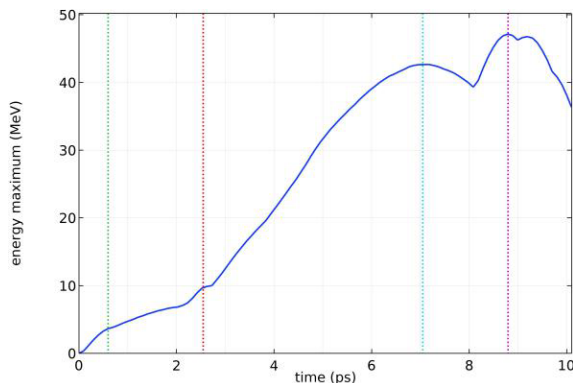

Figure 10. Electron distribution at 8.08 ps.

Figure 11. Electron energy maximum versus time.
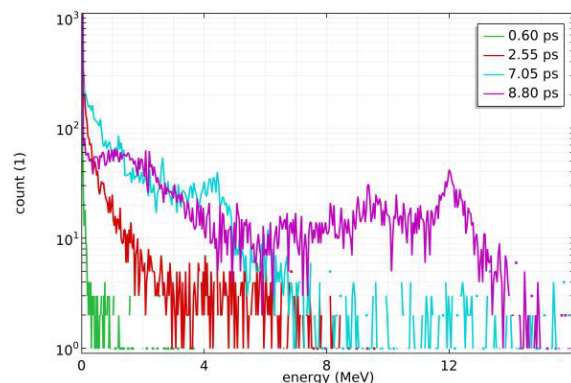
Figure 12. Energy spectra of electrons.
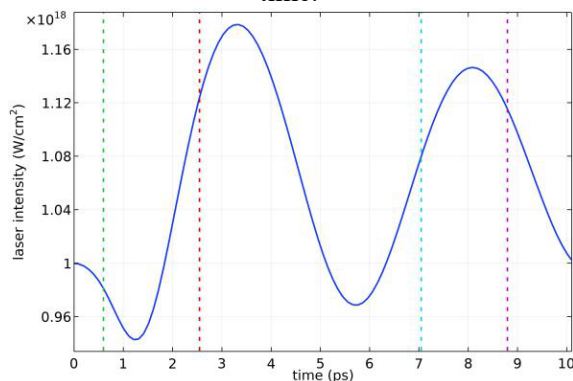
Figure 13. Axial intensity distribution of guided laser beam.
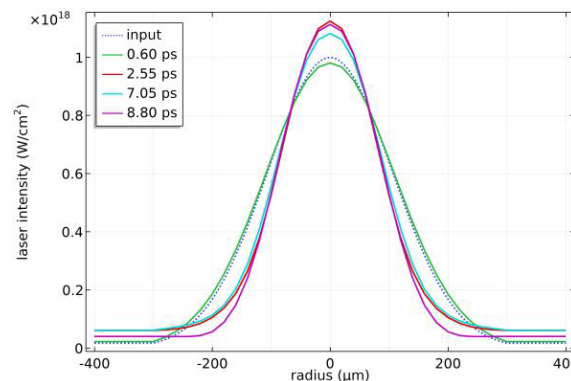
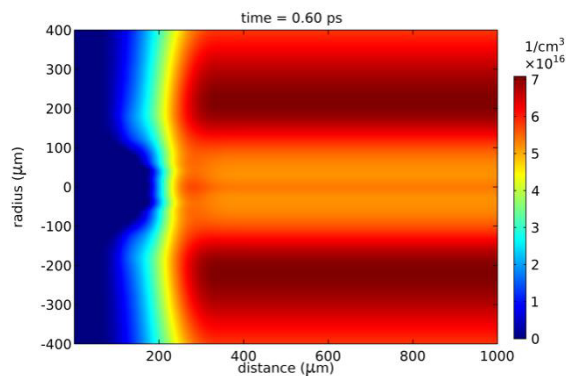**Figure 14.** Transverse intensity distribution of guided laser beam.
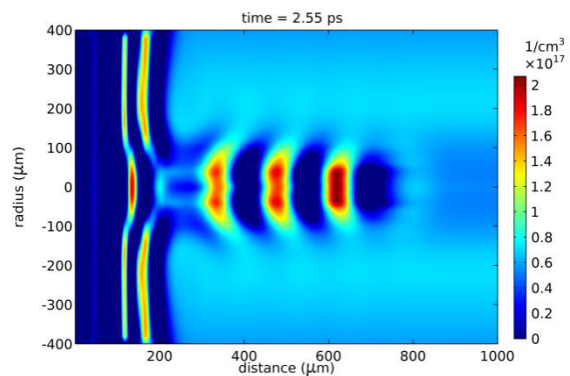
Figure 15. Electron density distribution at 0.6 ps.
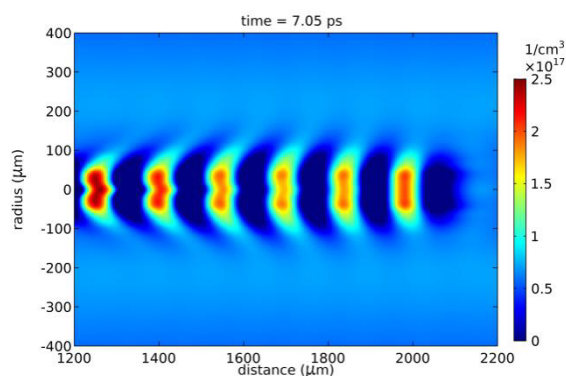

Figure 16. Electron density distribution at 2.55 ps.

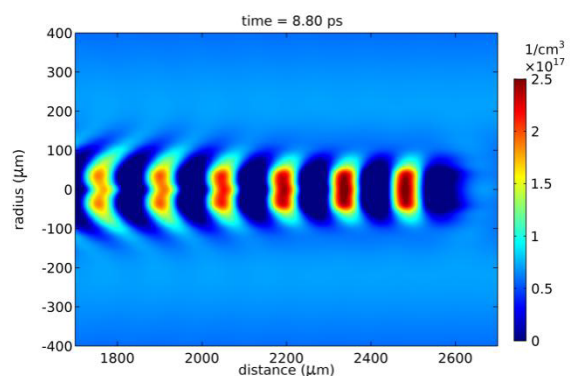**Figure 17.** Electron density distribution at 7.05 ps.
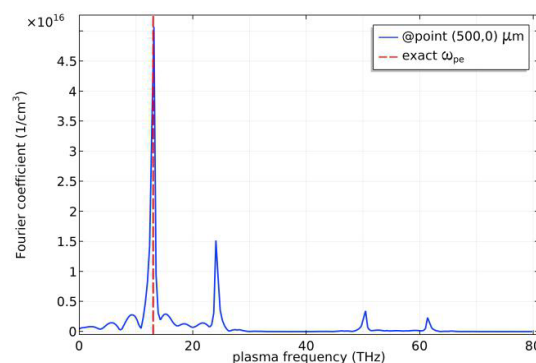

Figure 18. Electron density distribution at 8.80 ps.

Figure 19. The plasma density spectrum derived from plasma oscillations at point ($x = 500$ μm, $y = 0$ μm), where $\omega_{pe} = (e^2 n_e / \varepsilon_0 m_e \gamma)^{1/2}$ is the exact plasma frequency.

4. Summary and conclusion

The theoretical examination of the Z-pinch H-plasma waveguide inside a 3-mm inner diameter and 50-mm long capillary was performed on CO_2-laser pulse with input peak intensity of $>10^{15}$ W/cm^2. The main plasma variables of the fast Z-pinch discharge were computed by the 1-D MHD model. The waveguide properties of the capillary Z-pinch plasma were obtained from the space and frequency dependent wave equation that combines the attenuated charged particle inertia and the light wave effects in the plasma. Simulations showed that the guiding channel occurs far from capillary wall and exists for a few nanoseconds. In terms of laser driven plasma wakefield accelerators (LWFA), the Z-pinch waveguide is able to extend the acceleration length over the whole capillary. At the end of the guiding channel existence, the repetitive focusing and defocusing patterns were observed with intensity increase at the focal points. For simulation of the wakefield acceleration of electrons in the different waveguiding regimes, we used a PIC model. The influence of waveguiding regimes on the electron acceleration was demonstrated: quasi-synchronization of the electron energy maxima with the

inflection points between peaks of intensity of guided laser beam was demonstrated. We showed that the acceleration of electrons is nonlinear versus the acceleration time.

Acknowledgments

References

[1]   Tajima T and Dawson J M 1979 Phys. Rev. Lett. **43** 267
[2]   Sprangle P and Esarey E 1992 Phys. Fluids B Plasma Phys. **4** 2241
[3]   Ehrlich Y et al 1996 Phys. Rev. Lett. **77** 4186–4189
[4]   Kukhlevsky S V and Kozma L 1998 Contrib. Plasma Phys. **38** 583
[5]   Hosokai T et al. 2000 Opt. Lett. **25** 10
[6]   Hooker S M and Spence D J 2000 J. Opt. Soc. Amer. B Opt. Phys. **17** 90
[7]   Bobrova N A et al. 2001 Phys. Rev. E **65** 016407
[8]   Spence D J Butler A and Hooker S M 2003 J. Opt. Soc. Amer. B, Opt. Phys. **20** 138
[9]   Kumarappan V Kim K Y and Milchberg H M 2005 Phys. Rev. Lett. **94** 205004
[10]   Leemans W P et al. 2006 Nature Phys. **2** 696
[11]   Gordon D F 2007 IEEE Trans. Olasma Sci. **35** 1486
[12]   Gedde C G R et al. 2007 J. Phys., Conf. Ser. **78** 012021
[13]   Karsch S et al. 2007 New J. Phys. 9 415
[14]   A. J. Gonsalves et al. 2007 Phys. Rev. Lett. **98** 025002
[15]   Higashiguchi T et al. 2012 J. Appl. Phys. **111** 093302
[16]   Leemans W P et al. 2014 Phys. Rev. Lett. **113** 245002
[17]   Nakajima Ket al. 2015 High Power Laser Sci. Eng. **3** 11
[18]   Gonsalves A J et al. 2016 J. Appl. Phys. **119** 033302
[19]   Steinke S et al. 2016 Nature **530** 190
[20]   Luo J et al. 2018 Phys. Rev. Lett. **120** 154801
[21]   Zigler A et al. 2018 Appl. Phy. Lett. **113** 183505
[22]   Sasorov P V Bobrova N A and Olkhovskaya O G 2015 The two-temperature equations of magnetic hydrodynamics of the plasma (Moscow, Keldysh Institute Preprints) pp 1–18
[23]   Shapolov A A Kiss M and Kukhlevsky S V 2018 IEEE Transactions on Plasma Sci. **46** 3886